Electric field detection in laser-plasma interaction experiments via the proton imaging technique[a]

M. Borghesi[b]
Department of Pure and Applied Physics, The Queen's University of Belfast, Belfast BT7 1NN, United Kingdom

D. H. Campbell, A. Schiavi, and M. G. Haines
The Blackett Laboratory, Imperial College, London SW7 2BZ, United Kingdom

O. Willi
Institut für Laser und Plasmaphysik, Heinrich-Heine-Universität, Düsseldorf, Germany

A. J. MacKinnon and P. Patel
Lawrence Livermore National Laboratory, Livermore, California

L. A.Gizzi and M. Galimberti
Intense Laser Irradiation Laboratory, IFAM-CNR, 56100 Pisa, Italy

R. J. Clarke
Central Laser Facility, Rutherford Appleton Laboratory, Chilton OX11 0QX, United Kingdom

F. Pegoraro
Dipartimento di Fisica, Universitá di Pisa and INFM, Pisa, Italy

H. Ruhl
General Atomics, San Diego, California

S. Bulanov
General Physics Institute, RAS, Moscow, Russia

Due to their particular properties, the beams of the multi-MeV protons generated during the interaction of ultraintense ($I > 10^{19}$ W/cm^2) short pulses with thin solid targets are most suited for use as a particle probe in laser-plasma experiments. The recently developed *proton imaging* technique employs the beams in a point-projection imaging scheme as a diagnostic tool for the detection of electric fields in laser-plasma interaction experiments. In recent investigations carried out at the Rutherford Appleton Laboratory (RAL, UK), a wide range of laser-plasma interaction conditions of relevance for inertial confinement fusion (ICF)/fast ignition has been explored. Among the results obtained will be discussed: the electric field distribution in laser-produced long-scale plasmas of ICF interest; the measurement of highly transient electric fields related to the generation and dynamics of hot electron currents following ultra-intense laser irradiation of targets; the observation in underdense plasmas, after the propagation of ultra-intense laser pulses, of structures identified as the remnants of solitons produced in the wake of the pulse. © *2002 American Institute of Physics.* [DOI: 10.1063/1.1459457]

I. INTRODUCTION

Inertial confinement fusion (ICF) research has, on the one hand, driven the study of many important physical phenomena and, on the other hand, has led to the development of sophisticated diagnostics able to detect such processes. Diagnostic development is fundamental in order to face the continuous challenges presented by these studies. New diagnostics may lead to novel interpretations of known and unexplained physical phenomena, demonstrate phenomena predicted theoretically but not possible to observe with previously available diagnostics, or even highlight processes not predicted by present theory. This paper will present a novel diagnostic, proton imaging,[1] providing for the first time the possibility of diagnosing electric fields in dense plasmas and laser-irradiated targets, and therefore of contributing significantly to the advance of ICF studies. For example, the possibility of accessing directly electric field distributions in dense plasmas may shed new light on issues as hydrodynamic and electromagnetic instabilities highly detrimental for ICF. The technique has great potential for access to the complex and yet unexplored electromagnetic field distribution in indirect drive target assemblies. In a fast ignitor context, it can contribute to the study of the electron dynamics and transport following ultra-intense larger-plasma interactions, via detection of the ultralarge e.m. fields associated to the electron motion.

This paper will illustrate how the proton imaging diag-

nostic has been employed for the first time to study a number of dense plasma processes of interest to ICF, and in particular, to achieve the first electric field measurements in dense plasmas. The experiments have been carried out mainly using the VULCAN laser[2] at the Rutherford Appleton Laboratory (UK), but some tests have also been performed employing the JanUSP laser[3] at the Lawrence Livermore National Laboratory (CA).

II. EXPERIMENTAL PRINCIPLE AND PROTON PROBE PARAMETERS

This technique employs protons produced during ultraintense interactions[4] to probe, in a point projection imaging scheme, dense plasmas, and laser-irradiated targets. The proton beam cross-section profile and spectral content will in general undergo variations due to collisional stopping/scattering[5] and to deflection/slowing down due to electromagnetic fields. Therefore proton probing can be used as a diagnostic of the density variations encountered along the propagation direction of the beam. This type of diagnosis, generally called proton radiography,[6] has been pursued since the late 60s employing protons accelerated via conventional means (linear or cyclotron accelerators). Laser-produced protons have certainly great potential as a density diagnostic in thick targets, but this is not the subject of this paper. In the limit of thin targets (i.e., when probing targets with thickness much smaller than the collisional stopping distance for the protons employed), probe beam perturbation will be manly due to the e.m. fields present in or around the targets. The results presented in this paper have been obtained in this limit, and therefore the technique has been named proton imaging, both to distinguish it from what is conventionally called proton radiography and to indicate the intrinsic imaging properties of this diagnostic. As a matter of fact, the technique exploits the favorable characteristics of the multi-MeV proton beams emerging from the back of thin foils irradiated by high-intensity, short laser pulses.[4] There is presently a widespread interest in the study of the properties of these beams and the mechanisms originating them, and several recent papers deal with these issues both from an experimental and theoretical point of view.[4,7–9] Although the precise accelerating mechanisms are still the object of scientific debate, there is common agreement on the fact that the protons are accelerated by the electrostatic field set up by fast electrons propagating into or leaving the target.

Although some general characteristics are common to all experimental observations, the detailed properties of the beams depend on the parameters of the laser used to produce them and the characteristics of the targets employed, and careful programs of beam optimization are presently pursued by various groups. In the following, unless specifically declared, we will refer to the parameters of the proton beams obtained in the VULCAN laser experiments. This laser,[2] operating in the Chirped Pulse Amplification mode (CPA), provides 1.054 μm, 1 ps pulses with energy up to 100 J. When focused by an F/3.5 Off-Axis Parabola (OAP), the focal spot varied between 8 and 10 μm in diameter at full width at half maximum (FWHM), containing 30%–40% of the energy,
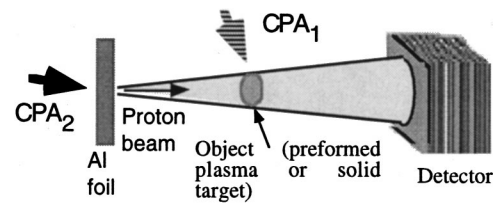

FIG. 1. Experimental setup for proton imaging. An intense laser pulse (CPA$_2$) was used to produce the proton beam. In part of the campaign a second CPA pulse (CPA$_1$) was available and focused on the object target in order to produce highly transient fields.

and giving intensities up to $(5-7)\times10^{19}$ W/cm^2. The targets used for proton beam production were Al foils, 1–2 mm wide and 3–25 μm thick. It should be remembered here that proton beams are observed even from metallic targets (in this case they originate from impurity layers on the target's surface[10]). The laser pulse was focused onto the center of the main target, at an angle of incidence of 15° with the target normal.

The proton beams produced under these conditions were bright, typically containing more than 10^{12} protons with energy above 3 MeV per shot.[9] The maximum energy of the protons typically reached about 25 MeV and their spectrum could be approximated by a Boltzmann exponential with T $\sim3-4$ MeV. The beams were highly directional, propagating along the normal to the back surface of the target with small angular divergence (the collimation increases with the energy, and the half-aperture of the beam is less than 15° above 10 MeV).

During the experiments the source size of the proton beam has been estimated using various methods, including penumbral edge techniques. At present we estimate that the source is smaller than 10 μm diameter for energies above 10 MeV. As we will also see in the next section, it is an issue if the observed source is real or rather a virtual one (with the protons emitted from a larger area, but with finite angular divergence and spread). In any case, the measured source size is small enough to permit the implementation of point projection imaging schemes, and sets the spatial resolution of the diagnostic.

The duration of the proton pulse at the source is predicted by the theory to be of the order of the pulse duration. Experimental evidence that it was below 5 ps has been obtained.

All of these properties are highly desirable if the proton beam is employed as a probe pulse. The idea of proton imaging is simple (see Fig. 1): as the proton beam originates (or appears to) from a small source, when a thin object is placed between the source and a detector, there will be a one-to-one correspondence between the points of the object plane and of the detector plane (we assume purely geometrical propagation for the protons). Distortions to this one-to-one correspondence can be ascribed to deflections undergone by the protons when crossing the object plane, and ultimately correlated to e.m. fields present in the object plane. The small source size and short duration ensure an intrinsically high spatial and temporal resolution for the diagnostic. Reaching

comparable spatial resolution with proton beams from conventional accelerators would require the use of sophisticated charged particle optics, while a ps temporal resolution is definitely beyond the possibilities of applications employing such pulses (which typically have duration in the ns range).

The detector employed in the whole campaign consisted of a stack of several layers of radiochromic (RC) film.[11] The film used (Gafchromic MD55) consists of 270 μm thick plastic continuing a double layer of organic dye, which reacts to ionizing radiation. The equivalent dose of energetic protons stopped in the film can be measured from the changes in optical density undergone by the film, yielding information on the number and energy of the protons. By using them in a stack, each layer of film acts as a filter for the following layers. Since protons deposit energy mainly in the Bragg peak at the end of their range, each RC film layer spectrally selects a narrow range of proton energies. Al filters of 25 μm were placed in front of the first layer of film giving a minimum detectable proton energy of about 3 MeV. Nuclear track detectors such as CR 39[12] were also used to insure that the signal observed on RC film was effectively due to protons (and not to electrons or x-rays).

As the detector can provide 2-D, spectrally resolved information about the proton intensity distribution across the beam cross-section, the broad spectral content of the beam does not represent a problem. It is actually an advantage when probing evolving field distributions. In fact, due to the different propagation velocity of the various energy components, the protons will be spread temporally when they reach the object plane. As the detector performs spectral selection, each layer will convey information pertaining to different stages of the target evolution. Therefore, as it will be seen later, the technique is intrinsically multiframe.

III. STATIC IMAGING AND SOURCE INVESTIGATION

If thick solid obstacles are placed in the beam, a shadow of the object is obviously produced in the proton beam, due to collisional stopping in the target. However, it was observed that a shadow forms even when objects with the thicknesses much smaller than the proton penetration depth were used, for example, 5–25 μm diameter Cu and Au wires. In particular, mesh arrays of wires were employed for a number of tests. The meshes were parallel to the main target, i.e., perpendicular to the proton beam.

The shadow of a mesh formed by 25 μm wires spaced by 100 μm is shown in Fig. 2(a), obtained with 20 MeV protons. The distance between the proton source and the mesh was $d=1$ mm, while the first of the radiochromic film layers was positioned at $L=22$ mm from the source. The optical density modulation observed is of the order of 0.2 [Fig. 2(b)]. The collisional stopping distance of 20 MeV protons in Cu is about 800 μm, and the collisional energy loss for such energetic protons in 25 μm of Cu is just $\Delta E/E \sim 2\times10^{-2}$. While such a variation is too small to explain the shadow, scattering of the protons crossing the mesh could account for the contrast variation observed,[6] and modeling is presently undergoing.
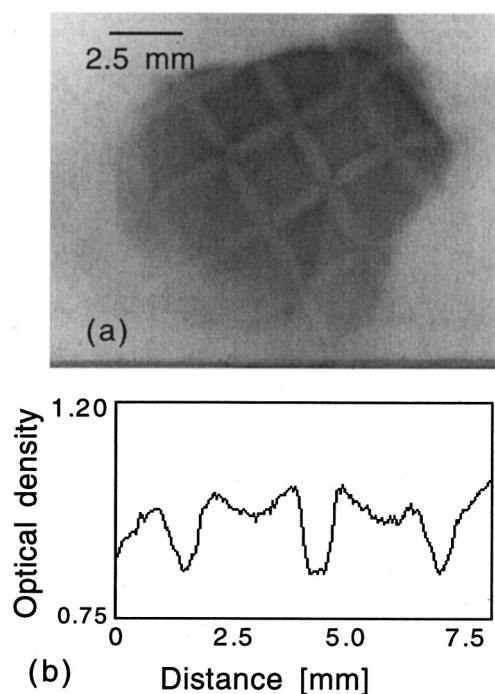

FIG. 2. (a) Shadow of a 25 μm wires mesh with 100 μm separation, obtained with 20 MeV protons onto RC film. (b) Lineout of optical density across the shadow.

The observation of the mesh magnification on the detector provides important information on the nature of the source. If the source was located at the plane of the target, the magnification would be given by $M_G = 1 + L/d$, with d and L, respectively, the source-to-object and object-to-detector distances. Detailed magnification tests were recently carried out using JanUSP.[3] It was seen that the experimental magnification M_{exp} is consistently lower than M_G. We believe that this may be due to the fact that the source is virtual and placed a distance x before the target. In this case the magnification would be given by $M_{exp} = 1 + L/(d+x)$ which is smaller than M_G. The deviation of the magnification observed experimentally from M_G is consistent with $x\sim400$ μm. This implies that the protons are emitted from a region of the target significantly larger than the apparent source size, but with a fixed divergence, in a laminar fashion. For example, taking an emittance half-angle of 15° (as observed for 10 MeV protons), the radius of the region emitting the protons would be around 100 μm.

IV. TRANSIENT FIELD MEASUREMENTS

The high temporal resolution of the diagnostic makes it ideal to study highly transient fields, such as, for example, the ones arising from the electron dynamics following intense, short pulse interactions. Such measurements were carried out by exploiting the possibility of splitting the VULCAN CPA pulse in two beams (CAP$_1$ and CPA$_2$), focusable with separate optics along separate lines. Due to setup constrains, the energy content of each pulse had to be limited to 20 J, giving intensities of about 10^{19} W/cm^2. The temporal separation of the two pulses could be varied on a shot-to-shot basis. The CPA$_2$ pulse was used to produce a proton beam
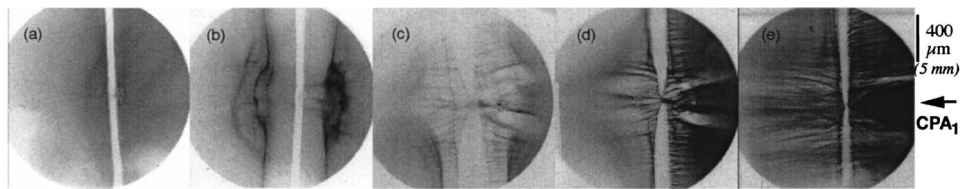
FIG. 3. Proton images of the interaction zone after irradiation with the CPA$_1$ pulse of a 50 μm Ta wire for different interaction-probing delays: (a) -15 ps; (b) -5 ps; (c) 5 ps; (d) 15 ps; (e) 25 ps. The energy of the protons employed was 6–7 MeV. Here and in the following figures spatial scales for both the target and the image plane (between bracket) are indicated.

from an Al foil, and the proton beam was used to probe, transversely, the interaction of the CPA$_1$ pulse with solid targets or preformed plasmas.

Particularly dramatic effects were observed probing the interaction of the CPA$_1$ pulse with small diameter metal wires. Figure 3 shows proton images of the interaction with a 50 μm Ta wire. The RC film layers shown (second layers of the RC stacks, corresponding to proton energies of 6–7 MeV) have been obtained in separate shots for different CPA$_1$–CPA$_2$ delays. When the proton probe arrived on target before the CPA$_2$ interaction pulse (e.g., $t = -15$ ps, first image in Fig. 3), only the shadow of the Ta wire, thick enough to slow down and scatter the protons is visible, with some small effect visible in the interaction region due to preplasma present ahead of the interaction. However, when the probe timing approaches the peak of the interaction pulse (second image of Fig. 3) a dramatic effect is observed, with the protons being deflected away from the surface of the wire, which charges up due to hot electron expulsion. The charge is seen to decay in a few tens of picoseconds, as filamentary structures (horizontal striations) are seen to appear. The onset of pronounced symmetrical horizontal features above and below the interaction axis is also detected. Such structures may be related to the radial expansion of shocks following the interaction, likely presenting non-neutral regions at their leading front.

From the proton deflection, quantitative information on the charging-up and discharge processes can be obtained. This is more easily done in an even simpler geometry. In Fig. 4 proton images taken after the ultraintense irradiation of a 150 μm glass micro-balloon are shown. The three images are obtained on three consecutive layers of RC in a single shot, and provide an example of the multiframe property of the diagnostic. In coincidence with the interaction, a shadow, much larger than the target, appears in the image, due to the proton deflection by the outwardly directed electric field. By matching the deflection to the calculated deflection for protons propagating in a Coulomb field,[13] we have obtained the first measurement of positive whole target charge-up due to the expulsion of fast electrons during the interaction.[14] The charge in Fig. 4(b) was estimated to be $Q \sim 2 \times 10^{-8}$ C. The corresponding electric field at the target surface is $E \sim 10^{10}$ V/m. A rapid discharge was observed.

On a comparable timescale, the onset of filamentary structures of the target surface is observed. The filamentary structures are first seen a few picoseconds after the peak of the interaction pulse, and appear as striations extending out-

wards along the normal to the target surface, even far away from the interaction region. This is clear in Fig. 4(b) where the filaments start to appear, and in Fig. 4(c), where they have fully grown. In Fig. 4(c) the filaments are seen both side-on and face-on (as a speckled pattern inside the shadow). The transverse wavelength of the modulation is about 10 μm and is more or less constant over the whole field of observation.

The observations are consistent with the growth, at the surface of the target, of an electromagnetic heat-flow instability,[15] arising in presence of two counterstreaming currents. The electrothermal instability,[16] which takes place in presence of counter-streaming flows of collisionless hot electrons and cold collisional electrons, is particularly relevant to our experimental conditions. In fact, such a situation will take place at the surface of the laser-irradiated target when some of the fast electrons ejected during the interaction flow back into the solid away from the focal spot region ("fountain effect"[17]), and an opposite cold electron current is drawn from the target to maintain neutrality. As the instability
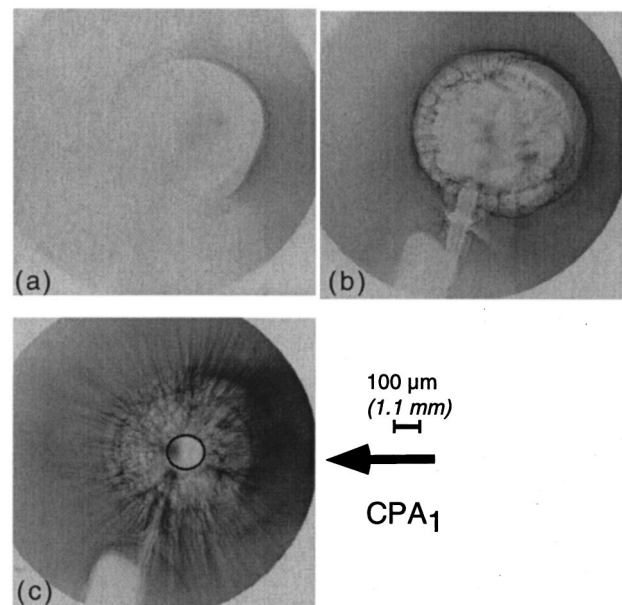

FIG. 4. Proton images taken following CPA; irradiation of a 150 μm glass micro-balloon. The original size and position of the target are indicated by the black circle in Fig. 4(c). Each picture refers to subsequent RC film layers (i.e., different proton energy Ep and different probing delay Δt from the interaction): (a) $Ep \sim 8$ MeV, $\Delta t \sim -3$; (b) $Ep \sim 6$–7 MeV, $\Delta t \sim 4$ ps; (c) $Ep \sim 3$–5 MeV, $\Delta t \sim 15$–20 ps.
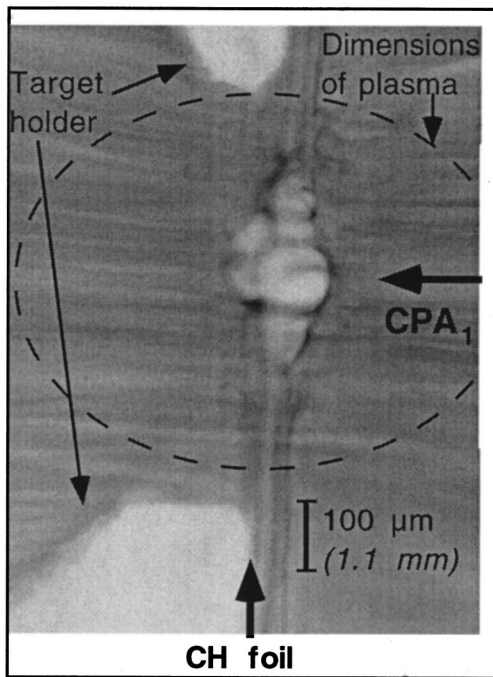
FIG. 5. (a) Proton image taken (using 8 MeV protons) 45 ps after the CPA$_1$ interaction with an underdense preformed plasma.

causes magnetized filamentation of both hot and cold currents, the effect is imprinted on the proton beam via the associated electric fields, transverse to the filaments. The instability grows at the target surface and the perturbations are transported out by the expanding plasma. Essentially the magnetic fields are frozen into the ablating plasma. Reference 16 provides order of magnitude scaling laws (which are independent from the intensity of the hot electron flux) for the growth rate α and the transverse wavelength λ of the modulation, i.e., $\alpha[s^{-1}] = 2.8 \times 10^{-8} \ n_0 Z/A T_e^{3/2}$, $\lambda[m] = 2.41 \times 10^{10} \ T_e^2 \sqrt{A}/n_0 Z$. n_0 and T_e are density and temperature of the cold electrons, Z and A charge and atomic number of the target material. For example, by using the density of solid glass ($n_0 \sim 5 \times 10^{28}$ m^{-32}), Z and A for Si (main constituent of the glass target) and $Te = 500$ eV, one obtains $\alpha^{-1} \sim 15$ ps and $\lambda \sim 5$ μm, of the order of the observations.

Proton probing of the field structures arising after the interaction of the ultraintense CPA$_1$ pulse with preformed plasmas was also carried out. The plasmas were produced by exploding thin plastic foil (0.3 μm thick) with two 1 ns, 0.527 μm laser pulses at a total irradiance of about 5 $\times 10^{14}$ W/cm^2. The delay between plasma formation and interaction was typically 1 ns.

The main feature observed in the proton images was the onset of several bubblelike structures following closely the interaction. A proton image of the plasma recorded 45 ps after the CPA$_1$ interaction, and obtained with 8 MeV protons, is shown in Fig. 5. Four to five bubblelike structures are clearly visible at the center of the plasma. A large structure with radius of approximately 50 μm is seen at the center of the picture, with other five smaller structures tightly packed around it. The structures are first observed in coincidence

with the interaction. No structures have been clearly observed at later times. The "bubbles" correspond to unexposed regions of the RC film, i.e., regions of the proton beam cross section from which protons have been evacuated. As the aerial density of the matter crossed by the beam is insignificant compared to the stopping range of the protons employed, it is reasonable to assume that the bubbles are observed in correspondence of plasma regions where localized electric field, with a component transverse to the proton propagation direction, are present. The region where the bubbles are present extend for about 300 μm in the transverse direction and for about 150 μm in the longitudinal direction. They are therefore observed even far away from the interaction axis and the vacuum focal spot region. It should be noted that in similar interaction conditions, break-up of the laser beam in several filaments diverging at wide angles has been observed.[18] This causes fractions of the laser energy to be spread as far as 150 μm from the propagation axis in the plasma central plane. It is therefore reasonable to assume that the spatial scale of the area occupied by the bubbles in the proton images is consistent with the dimension of the turbulent region left by the laser pulse in the central part of the plasma.

Spherical structures, which we believe can explain our observations, have been predicted by recently published particle-in-cell simulations. The simulations, studying the propagation of ultraintense laser pulses through underdense plasmas, have shown the appearance of a number of solitons in the wake of the laser pulse.[19] By solitons, here we mean small cavitated regions of plasma in which part of the e.m. radiation is trapped as an effect of frequency downshifting of the energy-depleted e.m. wave. These structures, originally with size of the order of the collisionless electron skin depth, tend to expand and merge together, originating "bubbles" substantially larger than the initial size (post-solitons).[20] The post-solitons contain a radial, outwardly directed, electrostatic field. The effect of this field on protons propagating through the bubbles will be to deflect them and create circularly shaped shadows in the proton density distribution as observed in the experiment. Analytical calculations, PIC and particle tracing simulations have been used to support this interpretation, and will be the subject of a forthcoming paper.[21] A first estimate, based on simple proton tracing arguments, of the maximum field inside the central bubble of Fig. 5 yields 5×10^9 V/m.

V. FIELD MAPPING IN LONG-SCALE PLASMAS

Proton probing can be employed as an important and novel diagnostic in conventional direct drive ICF. In order to investigate its potentialities, proton imaging of long-scale laser-produced plasmas of interest to ICF was also performed. The proton beam was produced as usual from a 25 μm Al foil, and the secondary target also consisted of a 25 μm Al foil. The plasma was formed by irradiating the 25 μm Al foil with a 527 nm laser pulse. The pulse had a flat-top intensity profile and duration of 600 ps. The pulse was focussed with an f/10 lens and the focal spot was modified from shot to shot in size and intensity profile by changing the
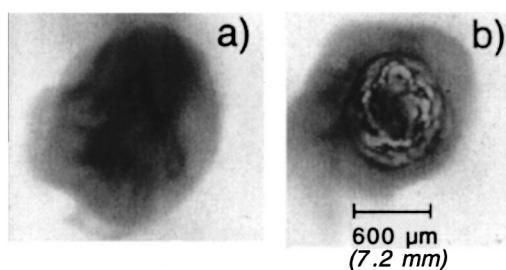
Phys. Plasmas, Vol. 9, No. 5, May 2002

Electric field detection in laser-plasma interaction . . .

2219

FIG. 6. Beam cross section for 17.6 MeV protons after propagation: (a) through a 25 μm Al coil foil, (b) through a long scale plasma formed by long pulse laser irradiation of the 25 μm Al foil.

focussing of the lens and by inserting phase zone plates (PZP) in the beam.[22] Typical irradiances on target were of the order of 10^{14}–10^{15} W/cm^2. Probing was performed both face-on and side-on (i.e., respectively, with the proton propagation axis parallel or perpendicular to the plasma symmetry axis). Additional information on the plasma was obtained via transverse interferometry measurements using a 266 nm laser beam with ps duration. Figure 6 presents two RC film layers corresponding to a proton energy of 17.6 MeV. Figure 6(a) shows a face-on image of a solid target with no plasma: the folding structures are due to the internal dynamics of the accelerating processes.[23] The presence of the target in the line of sight ins not detected because the areal density of a 25 μm Al foil is too low to affect significantly the ion beam. Figure 6(b) presents a face-on image taken at the peak of the plasma-forming laser pulse: in this case the protons going through the plasma are displaced or scattered by the e.m. fields present in the plasma. The recorded image clearly shows the footprint of these processes on the proton beam cross section. Comparison of these images with interferograms taken in similar conditions indicates that geometrical magnification holds for our imaging technique (within the limits pointed out in Sec. II). The structures and modulations imprinted on the ion beam must reflect the electromagnetic field distribution present in the plasma during the interaction, setup by electron motion under the effect of the laser pulse.

The temporal evolution of the observed structures was recorded by changing the delay between the plasma forming pulse and the CPA pulse. Images taken at the early stages of the laser interaction show the formation of these structures, which become fully developed toward the end of the pulse. Soon after the laser pulse is gone, the structures disappear and the image closely resembles the one when no plasma is present. Side-on images show that the structures extend from the solid density far out into the coronal region. When the irradiation conditions of the target were changed, distinct modifications on the recorded ion pattern were observed, indicating a close relationship between the fields experienced by the protons and the laser intensity profile. Face-on images show a fine structure made of cells, the size of which varies with the properties of the focal spot. The presence of a PZP introduces a fine-scale regular modulation on the laser profile, which is transferred to the e.m. fields structures inside the plasma and subsequently detected by the ion beam. As a

matter of fact, side-on shots also revealed a regular modulation in image intensity when PZPs are used.

Although several processes (laser imprint, heat-flow instabilities, parametric instabilities) can in principle be responsible for structures such as those mapped by the proton probe, it is presently unclear which amongst these is the dominant process. Modeling is presently undergoing with the aim of reconstructing the field distribution producing the structures observed, and individuate the dominant process causing them. Preliminary analysis using a 2-D charged-particle tracer, has been carried out. By assuming tubular E-field structures, like the ones that could be induced by laser hot spots, it has been found that E-fields of the order of 5×10^8 V/m are required to reproduce patterns similar to those observed.

VI. CONCLUSION

Proton imaging is a diagnostic with enormous potential for the investigation of fundamental plasma physics problems, which were difficult (or even impossible) to explore up to now. By using this diagnostic, for the first time measurements of transient electric fields in dense plasmas have been obtained, determining their evolution on a picosecond scale with micron spatial resolution. While extracting the field generating the proton pattern is relatively straightforward in simple geometries, the interpretation of more complex patterns, as those caused by propagation through long-scale laser-driven plasmas, will require use of numerical tools, including particle tracing, PIC, and hydrodynamic codes. Detailed analysis and modeling is presently undergoing.

ACKNOWLEDGMENTS

[1] See also M. Borghesi, A. Schiavi, D. H. Campbell, M. G. Haines, O. Willi, A. J. Mackinnon, L. A. Gizzi, M. Galimberti, R. J. Clarke, and H. Ruhl, Plasma Phys. Controlled Fusion **43**, A267 (2001).

[2] C. Danson, J. Collier, D. Neely et al., J. Mod. Opt. **45**, 1653 (1998).

[3] J. D. Bonlie, F. Patterson, D. Price, B. White, and P. Springer, Appl. Phys. B: Lasers Opt. **70**, S155 (2000).

[4] E. L. Clark, K. Krushelnick, J. R. Davies et al., Phys. Rev. Lett. **84**, 670 (2000); R. D. Snavely, M. H. Key, S. P. Hatchett et al., ibid. **85**, 2945 (2000).

[5] J. F. P. Ziegler, J. P. Biersack, and U. Littmark, The Stopping and Range of Ions in Solids (Pergamon, New York, 1996).

[6] A. M. Koehler, Science **160**, 303 (1968); D. West and A. C. Sherwood, Nature (London) **239**, 157 (1972); J. A. Cookson, Naturwissenschaften **61**, 184 (1974); N. S. P. King, E. Ables, K. Adams et al. Nucl. Instrum. Methods Phys. Res. A **424**, 84 (1999).

[7] S. P. Hatchett, C. G. Brown, T. E. Cowan et al., Phys. Plasmas **7**, 2076 (2000); S. M. Bulanov, N. M. Naumova, T. Zh. Esirkepov et al., JETP Lett. **71**, 407 (2000); Y. Sentoku, T. V. Lisseikina, T. Zh. Esirkepov et al., Phys. Rev. E **62**, 7271 (2000); S. Wilks, A. B. Langdon, T. E. Cowan, M. Roth, M. Singh, S. Hackett, M. H. Key, D. Pennington, A. J. Mackinnon, and R. A. Snavely, Phys. Plasmas **8**, 542 (2001); A. Pukhov, Phys. Rev. Lett. **86**, 3562 (2001); H. Ruhl, R. V. Bulanov, T. E. Cowan, T. V. Liseikina, P. Nickles, F. Pegoraro, M. Roth, and W. Sandner, Plasma Phys. Rep. **27**, 363 (2001); S. V. Bulanov, F. Califano, G. I. Dudnikova et al., in

2220   Phys. Plasmas, Vol. 9, No. 5, May 2002

Borghesi *et al.*

Reviews of Plasma Physics (Kluwer, New York, 2001), Vol. 22, p. 227.

[8] A. Maksimchuk, S. Gu, K. Flippo, D. Umstadter, and V. Yu. Bychenkov, Phys. Rev. Lett. **84**, 4108 (2000).

[9] A. J. Mackinnon, M. Borghesi, S. Hatchett, M. H. Key, P. Patel, D. H. Campbell, A. Schiavi, R. Snavely, and O. Willi, Phys. Rev. Lett. **86**, 1769 (2001).

[10] S. J. Gitomer, R. D. Jones, F. Begay, A. W. Ehler, J. F. Kephart, and R. Kristal, Phys. Fluids **29**, 2679 (1986).

[11] W. L. C. McLaughlin, J. C. Humphreys, D. Hocken, and W. J. Chappas, Nucl. Instrum. Methods Phys. Res. A **302**, 165 (1991).

[12] A. P. Fews and D. L. Henshaw, Nucl. Instrum. Methods Phys. Res. **197**, 512 (1982); A. P. Fews, Nucl. Instrum. Methods Phys. Res. B **71**, 465 (1992).

[13] O. Kemperer, *Electron Physics* (Butterworths, London, 1972).

[14] M. Borghesi, D. H. Campbell, M. G. Haines *et al.*, ''Detection of highly transient electric fields with multi-MeV laser-produced proton beams,'' Nature (submitted).

[15] M. H. Key, ''Compression and hydrodynamics,'' in *Laser–Plasma Interactions 3* (The Scottish Universities Summer School in Physics, Edinburgh, 1985), p. 29.

[16] M. G. Haines, Phys. Rev. Lett. **47**, 917 (1981).

[17] R. Kolodner and E. Yablonovitch, Phys. Rev. Lett. **43**, 1402 (1979).

[18] M. Borghesi, D. H. Campbell, M. Galimberti, L. A. Gizzi, A. J. Mackinnon, W. Nazarov, A. Schiavi, and O. Willi, Proc. SPIE **4424**, 414 (2001); M. Galimberti, A. Giulietti, D. Giulietti, L. A. Gizzi, M. Borghesi, D. H. Campbell, A. Schiavi, and O. Willi, *ibid.* **4424**, 512 (2001).

[19] S. V. Bulanov, T. Zh. Esirkepov, N. Naumova, F. Pegoraro, and V. A. Vshivkov, Phys. Rev. Lett. **82**, 3440 (1999); Y. Sentoku, T. Zh. Esirkepov, K. Mima, K. Nishihara, F. Califano, F. Pegoraro, H. Sakagami, Y. Kitagawa, N. M. Naumova, and S. V. Bulanov, *ibid.* **83**, 3434 (1999).

[20] N. M. Naumova, S. V. Bulanov, T. Zh. Esirkepov, D. Farina, K. Nishihara, F. Pegoraro, H. Ruhl, and A. S. Sakharov, Phys. Rev. Lett. **87**, 185004 (2001).

[21] M. Borghesi, S. V. Bulanov, D. H. Campbell *et al.*, Phys. Rev. Lett. (to be published).

[22] T. H. Bett, C. N. Danson, P. Jinks, D. A. Pepler, and I. N. Ross, Appl. Opt. **34**, 4025 (1995).

[23] T. E. Cowan, M. M. Allen, I. Barton *et al.*, Bull. Am. Phys. Soc. **46**, 254 (2001).